WILEY | Hindawi

Research Article

Noise Estimation and Type Identification in Natural Scene and Medical Images using Deep Learning Approaches

G. Kavitha [iD],[1,2] **Chetana Prakash** [iD],[1] **Majid Alhomrani** [iD],[3,4] **N. Pradeep** [iD],[1]
Abdulhakeem S. Alamri [iD],[3,4] **Piyush Kumar Pareek** [iD],[5] **and Musah Alhassan** [iD][6]

[1]*Department of Computer Science and Engineering, Bapuji Institute of Engineering and Technology, Davangere 577004, Karnataka, India*
[2]*Department of Computer Science and Engineering, University BDT College of Engineering, Davangere 577004, Karnataka, India*
[3]*Department of Clinical Laboratories Sciences, The Faculty of Applied Medical Sciences, Taif University, Taif, Saudi Arabia*
[4]*Centre of Biomedical Sciences Research (CBSR), Deanship of Scientific Research, Taif University, Taif, Saudi Arabia*
[5]*Department of Computer Science and Engineering and Head of IPR Cell, Nitte Meenakshi Institute of Technology, Bengaluru, India*
[6]*University for Development Studies, Tamale, Ghana*

Correspondence should be addressed to Musah Alhassan; musahalhassan@uds.edu.gh

The image enhancement for the natural images is the vast field where the quality of the images degrades based on the capturing and processing methods employed by the capturing devices. Based on noise type and estimation of noise, filter need to be adopted for enhancing the quality of the image. In the same manner, the medical field also needs some filtering mechanism to reduce the noise and detection of the disease based on the clarity of the image captured; in accordance with it, the preprocessing steps play a vital role to reduce the burden on the radiologist to make the decision on presence of disease. Based on the estimated noise and its type, the filters are selected to delete the unwanted signals from the image. Hence, identifying noise types and denoising play an important role in image analysis. The proposed framework addresses the noise estimation and filtering process to obtain the enhanced images. This paper estimates and detects the noise types, namely Gaussian, motion artifacts, Poisson, salt-andpepper, and speckle noises. Noise is estimated by using discrete wavelet transformation (DWT). This separates the image into quadruple sub-bands. Noise and HH sub-band are high-frequency components. HH sub-band also has vertical edges. These vertical edges are removed by performing Hadamard operation on downsampled Sobel edge-detected image and HH sub-band. Using HH sub-band after removing vertical edges is considered for estimating the noise. The Rician energy equation is used to estimate the noise. This is given as input for Artificial Neural Network to improve the estimated noise level. For identifying noise type, CNN is used. After removing vertical edges, the HH sub-band is given to the CNN model for classification. The classification accuracy results of identifying noise type are 100% on natural images and 96.3% on medical images.

1. Introduction

Digital images are part of everyday life. Applications such as satellite television, medical imaging, geographic information systems, and astronomy use digital images. Regarding the information revolution, one of the most intriguing features is the capacity to communicate and receive sophisticated data beyond traditional written language boundaries. In images, noise modeling is influenced by the capturing instruments and by problems with the data acquisition process. Other factors that influence noise modeling in images include radiation sources, transmission media, and image quantization.

An image is defined as a function with two dimensions $f(x_i, y_i)$ x_i and y_i are coordinates and $f(x_i, y_i)$ is the gray value. There are two types of images: grayscale image with one gray channel and RGB image with red, green, and blue channels.

Many medical imaging modalities are available. Ultrasound or sonogram is the cheapest and safest medical
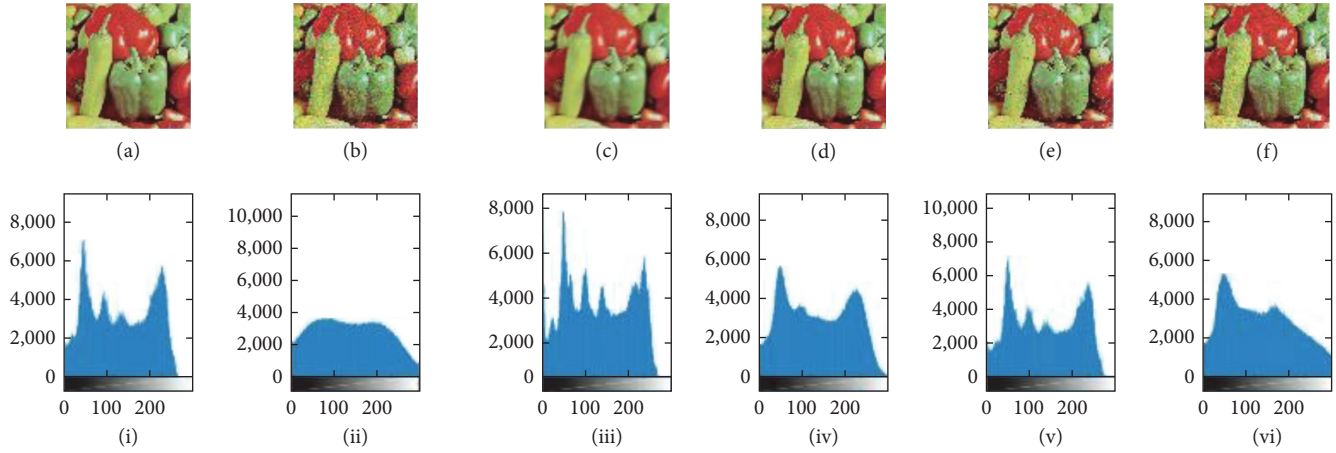
FIGURE 1: (a) Natural image, (b) Gaussian noised image, (c) motion noised image, (d) Poisson noised image, (e) salt-and-pepper noised image, (f) speckle noised image, (i) histogram of (a), (ii) histogram of (b), (iii) histogram of (c), (iv) histogram of (d), (v) histogram of (e), and (vi) histogram of (f).
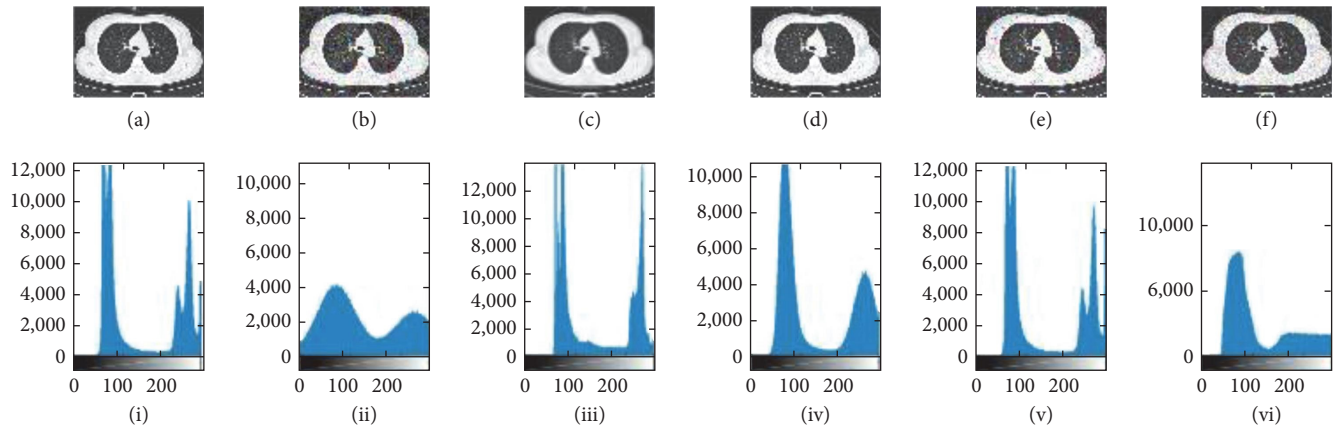

FIGURE 2: (a) CT image, (b) Gaussian noised image, (c) motion noised image, (d) Poisson noised image, (e) salt-and pepper noised image, (f) speckle noised image, (i) histogram of (a), (ii) histogram of (b), (iii) histogram of (c), (iv) histogram of (d), (v) histogram of (e), and (vi) histogram of figure (f).

imaging for investigating abdominal and pelvic organs and checking fetal development. CT is costlier than the US and more affordable than MRI. They detect tumors, bone fractures, cancer identification, and internal bleeding. MRI is used to capture images of anatomical and physiological body regions. In all these imaging modalities, during its acquisition process, noise increases because of the capturing procedure, electrical fluctuations, body movement, body fat, and liquid present in the body. For example, in asymptomatic diseases such as brain aneurysms in their first stage, their features are similar to pixels of white noise. If missed during MRI imaging, it results in subarachnoid hemorrhage (SAH). SAH discharges blood into the subarachnoid space, it has 40% risk of life threatening [1]. A noisy image may not detect aneurysm leading to human mistakes in its detection. Similarly, the presence of noises reduces the performance of segmentation, registration, classification, or tensor estimation [2]. MR images get noise due to scanned objects, electrical fluctuations during acquisition, noise due to RF coils and conductors, and hardware components [3]. Noises in MRIs are often considered as Racian distribution with

low levels (SNR < 2) [4] and the Gaussian distributions with SNR > 2 [5]. For denoising, many filters such as spatial domain filters, transform domain filters, anisotropic filters, nonlocal means, and wavelet transform approaches are used [6–9].

The noise unfavorably affects the image quality and may also damage postimage processing procedures. For improved observation and analysis of medical images, noise estimation, type identification, denoising, and image augmentation becomes crucial. Noise's standard deviation is estimated and used as image denoising parameters and thereby improving images' visual quality. Thus, the noise type should be predicted to generate denoised images. Several methods are present to eliminate noise, but there is a need for accurate noise estimation and its type identification. Figures 1(a) and 2(a) are original images of natural and medical image datasets, respectively.

Type of the noises:

(1) Gaussian noise is the random intensity values added to the image, and it occurs when the random

TABLE 1: Literature survey summary.

| References	Methodology	Dataset	Performance measure and accuracy	Gaps identified
[17]	Noise identification and denoising from the grayscale image; Noise: impulse noise	Dataset: Baboon, Cameraman, Lena, peppers, and Pemaquid images (512 × 512 image resolution)	Accuracy: PSNR = 47.278, SSIM = 0.978, SDME = 61.637	The image size is only five; Identify only noisy pixels
[29]	Noises: impulse and electronic; Statistical features: kurtosis and skewness fed to the ANN	Dataset: Kaggle dataset of natural images; Two hundred images of both noises. Training 60%, testing 40%	Accuracy 94.37%	Lesser number of images are considered for training and testing
[13]	Noises: Gaussian; Estimate noise level using DWT coefficients	Dataset: MRI images of T1 and T2 weighted	Estimate noise	No classification
[30]	Noise: Gaussian, speckle, line pattern stripes, and circle pattern ring; Two-cascaded CNN model is designed	BSD dataset and 1,000 CT dataset from NBIA, 300 SEM dataset from Dartmouth	Performance measure: PSNR and SSIM; PSNR-37.46, SSIM-0.9001	They are estimating the noise and denoising using CNN
[28]	Noises: impulse, Gaussian, speckle, and Poisson; To reduce the computation time, the PCA filters are used	Dataset: natural images from SIPI dataset–misc	We have carried out three experiments. Four types of noise combinations of noises; Overall accuracy 86.3%	They are considered four types of noise impulse, Gaussian, speckle, and Poisson, with eight classifiers
[14]	Noise: impulse; DCT to obtain the kurtosis in terms of a sum of absolute deviation to identify impulse noise	Dataset: natural images USC-SIPI Image database; Size 170 images of different noise levels	Accuracy: 97%	The data set is small and natural images. Considers only impulse noise
[15]	Noise: Gaussian, Speckle, and salt and pepper; Statistical features such as kurtosis and skewness	Dataset: few images from natural and medical	Features: kurtosis, skewness; Accuracy: not given	Few images
[16]	Noises: Gaussian, speckle, salt-and-pepper; Features: kurtosis and skewness. Method: PNN	Dataset: natural images; Size: not mentioned	Accuracy: 82%	NA
[31]	Gaussian, speckle, salt-and-pepper; Features: kurtosis and skewness. ANN for classification	Dataset: natural images; Size: 180 images	Accuracy: average 84%	NA
[32]	Noises: Gaussian, speckle, salt-and-pepper; Features: kurtosis and skewness. Method: KNN, NN	Dataset: natural images; Size: 70	Accuracy: ANN: 87%, NN: 90%	Seventy natural images such as cameraman are used
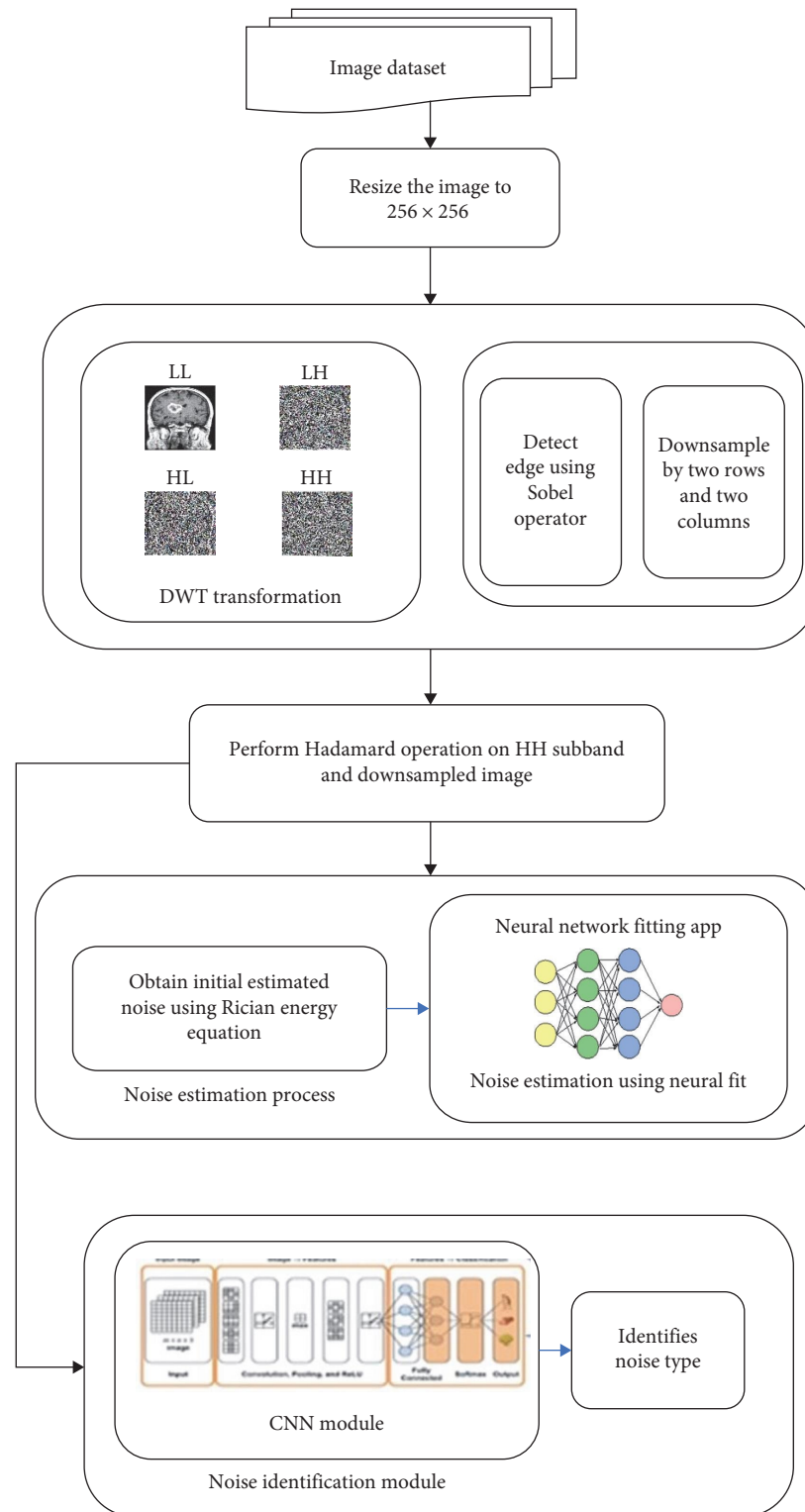
FIGURE 3: A proposed system for noise estimation and noise type identification.

fluctuations from the source happen. On natural or medical images, it degrades the image by masking the fine details of the image. Figures 1(b) and 2(b) show their effect on natural and medical images.

(2) Motion artifact: a noise that adds to the image during the acquisition of the image because of patients' movement of fluids in the body and breathing. This blurs the image by smudging the boundaries. Figures 1(c)
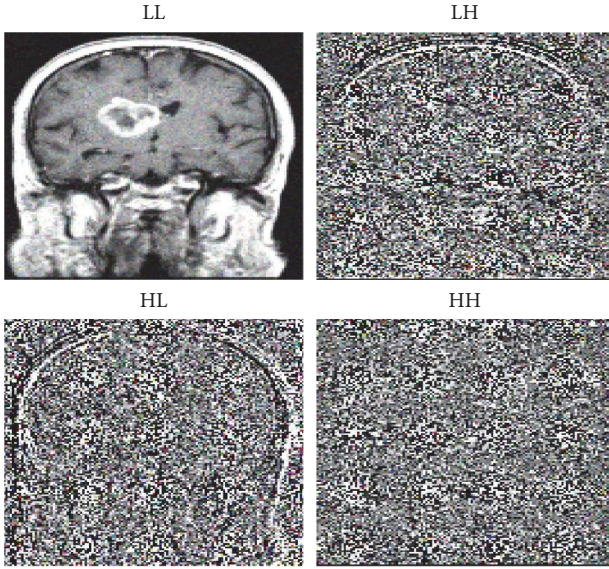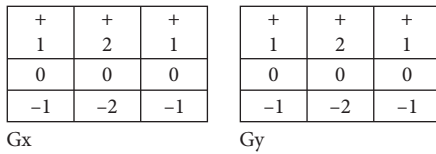
LL LH
HL HH

FIGURE 4: DWT components of the image.

+	+	+		+	+	+
1	2	1		1	2	1
0	0	0		0	0	0
−1	−2	−1		−1	−2	−1

Gx Gy

FIGURE 5: Sobel operator.

Combination of Sobel and HH component

FIGURE 6: Hadamard operated image.

TABLE 2: Training framework for neural fit model for both medical and natural scene images.

Parameters	Descriptions
Hidden layer	10
Algorithm	Levenberg–Marquardt backpropagation
Learning rate	1×10^{-4}
Total number of images	1,800
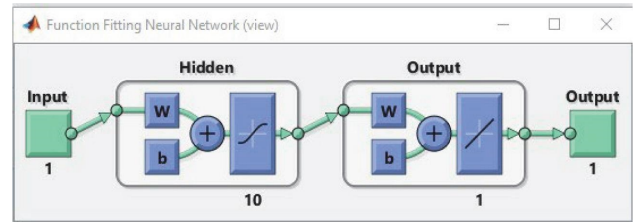
FIGURE 7: Model design for estimating noise.

and 2(c) show their effect on natural and medical images.

(3) Shot noise or Poisson noise: modeled using the Poisson process. This adds up to the image from the electric fluctuations. This is also similar to Gaussian noise. Figures 1(d) and 2(d) show their effect on natural and medical images.

(4) Salt-and-pepper noise or impulse noise: may be created by small and unexpected disturbances in the image signal. It expresses itself by randomly occurring white or black (or both) dots over the image. On the natural or medical images, it appears as sparsely appearing black and white spots, which may vanish the micro details of the image. Figures 1(e) and 2(e) show their effect on natural and medical images.

(5) Speckle noise is represented as multiplicative values. This adds to the image from the interference of many waves of the same frequency. This also appears same as Gaussian noise. Figure 1(e) and 2(f) show their effect on natural and medical images.

Effects of the noises on the medical images:

(1) The detection of the boundary of the objects becomes tough when the noises are present in the image

(2) Due to the wrong placement of the boundaries, the area measurements of tumors or any other clinical measure give the wrong results
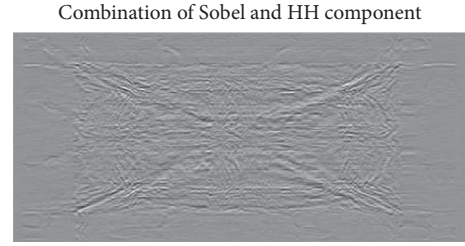
(3) The contrast and angle changes in the images can introduce the more complexity in differentiating between the healthy and unhealthy cells

On natural scene images:

(1) The noise factors on the natural image make the machine learning model to give the wrong decisions.

(2) While training the machine learning model for the object detection needs the clearer images. Noised images may train the system wrongly thereby whole model goes wrong.

In the machine learning approaches, the accuracy of the model depends on the feature-choosing methods, if the choice of features goes wrong the accuracy of the model is affected. Whereas in the deep learning model, the feature selection is automatic, based on the images of the dataset the features are selected which enhance the correctness of the model. Hence, the deep learning model provides the higher results compared to the machine learning models.

Highlights of this paper are:

(1) Noise present in the medical image is estimated initially using the Rician energy equation and then refined using the neural fit model.

TABLE 3: Training parameters for CNN model for both medical images and natural scene images.

Parameters	Descriptions
Input layer	$112 \times 112 \times 1$
First layer	Filter kernel size is 3×3 with 8 filters with padding.
Batch normalization and ReLU layer	
Second layer	Kernel size is 3×3 with 16 filters with padding
Batch normalization and ReLU layer	
Third layer	Kernel size is 3×3 with 32 filters with padding
Batch normalization and ReLU layer	
Fourth layer	Kernel size is 3×3 with 32 filters with padding
Softmax	Fitting tool
Learning rate	1×10^{-4}
Validation frequency	30

(2) A novel CNN approach is designed to identify the noise type. The accuracy of classification is 100%.

(3) The same approach is applied to medical images. Obtained accuracy of classification is 96.3%.

2. Literature Survey

Noise estimation is performed in the spatial and transformation domain. Spatial domain noise is estimated using PCA [10], a fuzzy model in MRI images [11]. In transformation, domain noise is estimated using DWT coefficients [12]. Both spatial and transformation domain are used to find the noise amount [13].

The presence of noise was identified by applying the DCT to obtain the kurtosis. The kurtosis values decrease with an increase in the noise density. The threshold value is computed by observing the kurtosis value for every image in the dataset. The absolute deviation for the noisy and noise-free images is calculated to decide image is noisy or not. They have considered the SIPI MISC dataset of natural images. The noise type detected is impulse, achieving an accuracy of 97% [14]. Subashini and Bharathi [38] extracted the statistical features such as kurtosis and skewness to determine the Gaussian, speckle, and salt,-and-pepper noises using the minimum distance pattern classifier. The experiment is conducted on satellite, X-ray, MRI, and digital images [15]. The Gaussian and impulse noise identification and removal by using the intensity equalization technique where the author calculates the distance between the histograms, the maximum distance becomes the threshold depending on the value of the type of noises identified the noises and the adaptive filters are employed to remove the noises [16]. Kumar and Nagaraju [17] designed a methodology to denoise the grayscale image by collecting the features such as entropy, information gain, and skewness and carried out a comparative analysis on the six classifiers and achieved the PSNR, SSIM, and SDME values of 47.27, 0.97 and 61.63 dB, respectively. The regression methods such as the kernel greedy algorithm are employed to detect the Gaussian noise using the orthogonal matching pursuit algorithm and achieve a mean square error of 0.033 [18]. The speckle noise is determined using the CNN, which has the two cascaded CNN models designed.

The first stage will estimate the noise and give the input to the second module along with the noise image to remove the noise. Four layers in both the sets of CNN are designed with input dimension $40 \times 40 \times 3$. The dataset: 1,000 CT images of size 256×256 (National Biomedical Imaging Archive) is employed and achieved the PSNR of 23.05 [19]. To estimate the presence of noise, a fuzzy model and DWT coefficients are used [20, 21]. Very few authors have contributed in identifying noise type. Most of the authors concentrate on denoising the specific type of noised images [10, 22–27].

The CNN model is employed to identify the noises such as impulse, Gaussian, and Poisson noises. They have used the SIPI MISC natural image dataset, noised with one and multiple combinations of noises of the dataset size 12,650 image, for training 11,000 and testing 1,650. To reduce the computation time, PCA filters are used at every layer; 21 layers are present in the model and achieved an overall accuracy of 96.3% [28]. Table 1 represents the literature review summary.

2.1. Summary of Literature Survey. The nature of the noise is preassumed based on the imaging modality used. These assumptions have saturated the performance of the filters. Many of the authors have proposed different techniques to identify impulse noise in a window of varying sizes. Very few authors have contributed to identify the noise type of the image. Dataset used is of natural images, and size is less. Hence, there is a need for detecting noise type of an image. After identifying noise type, a better denoising technique can be applied. Knowing the nature and distribution of noise plays a vital role. Hence, it is essential to characterize the noise type and noise level present in the images.

3. Proposed Methodology

The proposed approach for estimating noise and identifying noise types is shown in Figure 3. It has four main parts: the input image is transformed into DWT coefficients in the first part. The second part detects the edges from the input image and then down samples. The third part estimates the noise, and the fourth part identifies the noise type. The proposed algorithm for noise estimation and identification is shown in Algorithms 1 and 2.

Input: Noised images
Output: Estimated noise level
Method:
Step 1: Read images
      For $i = 1$ to n do
            Read image I_i
            Repeat step 2 to 5 for each image
Step 2: Resize an image
            Resize image I_i to 256×256
Step 3: DWT transformation
            $[LL, LH, HL, HH] =$ DWT transformation.
Step 4: Edge detection and reduce size to match with HH sub-band
            $I_d =$ Detect edges of I_i using the Sobel
              operator.
            $I_{dd} =$ Downsample the image by two rows and
              two columns.
Step 5: Remove edge component from HH sub-band
            $I_{we} = HH \bigcirc I_{dd}$ Hadamard operation
Step 6: Estimate noise level
            Initial noise level = Using Equation 3.
            Create a csv file with 2 column: estimated
              noise level and label.
Step 7: Train and test the neural fit model
            Divide csv file in the ratio $70 : 15 : 15$.

ALGORITHM 1: Proposed algorithm for noise estimation.

Input: Noised images
Output: Identified noise type
Method:
Step 1: Read images
      For $i = 1$ to n do
            Read image I_i
            Repeat step 2–5 for each image
Step 2: Resize an image
            Resize image I_i to 256×256
Step 3: DWT transformation
            $[LL, LH, HL, HH] =$ DWT transformation.
Step 4: Edge Detection and reduce size to match with HH
    sub-band
            $I_d =$ Detect edges of I_i using the Sobel
              operator.
            $I_{dd} =$ Downsample the image by two rows
              and two columns.
Step 5: Remove edge component from HH sub-band
            $I_{we} = HH \bigcirc I_{dd}$ Hadamard operation
Step 6: Train and test the CNN model using the images
    obtained in step 5
            Divide images in the ratio $60 : 20 : 20$.
Step 7: Measure the performance.

ALGORITHM 2: Proposed algorithm for noise type identification.

3.1. Noise Estimation. Using the high-frequency components of the image noise is estimated. HH sub-band obtained from DWT has high-frequency components as well as diagonal edges. Diagonal edges are important features of the images; hence, they are not noises. So, these diagonal features have to be subtracted from the sub-band. For this, the borders of the whole image are found using the Sobel and then down-sampled by 2. In order to remove diagonal edges, Hadamard operation is performed. Initial noise level of this image is determined utilizing noise using the Rician energy equation and then fed to the neural fit method to improve the estimated noise accuracy and resilience even more.

The blocks of the proposed system are briefed in this subsection.

3.2. Wavelet Transformation. The wavelet transform's fundamental technique uses a function whose initial wavelet is zero. The fundamental wavelet may be expanded and translated to provide a function. The expression of the Haar wavelet and the scaling factor equation are as shown in Equation (1). The components are shown in Figure 4.

$$\varphi_k^{(x)} = \left\{ \begin{array}{c} 10 \leq x \leq 0.5 - 1 \\ 0.5 \leq x < 10 \end{array} \right\}. \qquad (1)$$

3.3. Edge Detection using Sobel Operator. Sobel filter is a basic approximation to the notion of a gradient with smoothing. The gradients in the X and Y axes are often detected using the 3×3 convolution mask. The operator consists of a pair of 3×3 kernels, as shown in Figure 5.

The kernels may be applied individually on the input image to obtain gradient components (name them G_x and G_y). The size and direction of the gradient at each position may be determined by combining these values using Equation (2).

$$G = \sqrt{G_x^2 + G_y^2}, \qquad (2)$$

where G is the gradient value, G_x and G_y are the gradient components, respectively.

3.4. Initial Noise Estimation. After applying wavelet transform, HH sub-bands standard deviation is found using Rician energy equation Equation (3).

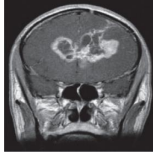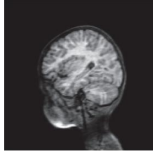$$\sigma_{ne} = \frac{\sqrt{k}}{N} \sqrt{\sum_{i,j \epsilon HH} J_{ne}^2(i,j)}, \qquad (3)$$
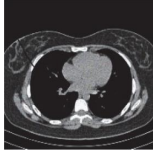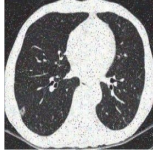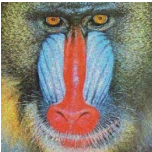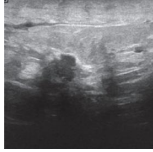
where σ_{ne} is the standard deviation of the noisy HH sub-band without edge, k is the constant equal to 4, N is the size, and J_{ne} is the nonedge image. The combined image of Sobel and HH sub-band obtained image is shown in Figure 6.

3.5. Noise Estimation using Neural Fit. The purpose of the proposed system is to perform the noise estimation using the

TABLE 4: Description of data acquisition.

S. no.	Noise type	No. of natural images	No. of medical images
1.	Gaussian	44 images with noise levels:1%, 2%, 3%, 4%, and 5%	109 images with noise levels:1%, 2%, 3%, 4%, and 5%
2.	Motion	44 images with noise levels:1%, 2%, 3%, 4%, and 5%	118 images with noise levels:1%, 2%, 3%, 4%, and 5%
3.	Poisson	44 images with noise levels:1%, 2%, 3%, 4%, and 5%	71 images with noise levels:1%, 2%, 3%, 4%, and 5%
4.	Salt-and-pepper	44 images with noise levels:1%, 2%, 3%, 4%, and 5%	139 images with noise levels:1%, 2%, 3%, 4%, and 5%
5.	Speckle	44 images with noise levels:1%, 2%, 3%, 4%, and 5%	141 images with noise levels:1%, 2%, 3%, 4%, and 5%
Total images		1,100	2,890

TABLE 5: Sample images from the dataset.

Name of the noise	Natural images from SIPI database	Medical images from TCIA and local hospitals
Gaussian noise		
Motion artifacts		
Poisson		
Salt-and-pepper		
Speckle noise		

Rician energy equation and neural fit [33]. The initial noise is found by using Equation (3). For the adaptive noise estimation, the Rician noise is employed, and it is applied to the HH subcomponent [21].

The neural tool MATLAB is employed to design the neural fit model. The GUI-based training model has ten hidden layers, a sigmoid activation function, and a feed-forward network [34]. The features are divided into 60, 20, and 20 for the training, testing, and validation. The Levenberg–Marquardt algorithm is used for training with 10 hidden layers. The error is measured using mean square error. The parameters involved in training are as shown in Table 2.
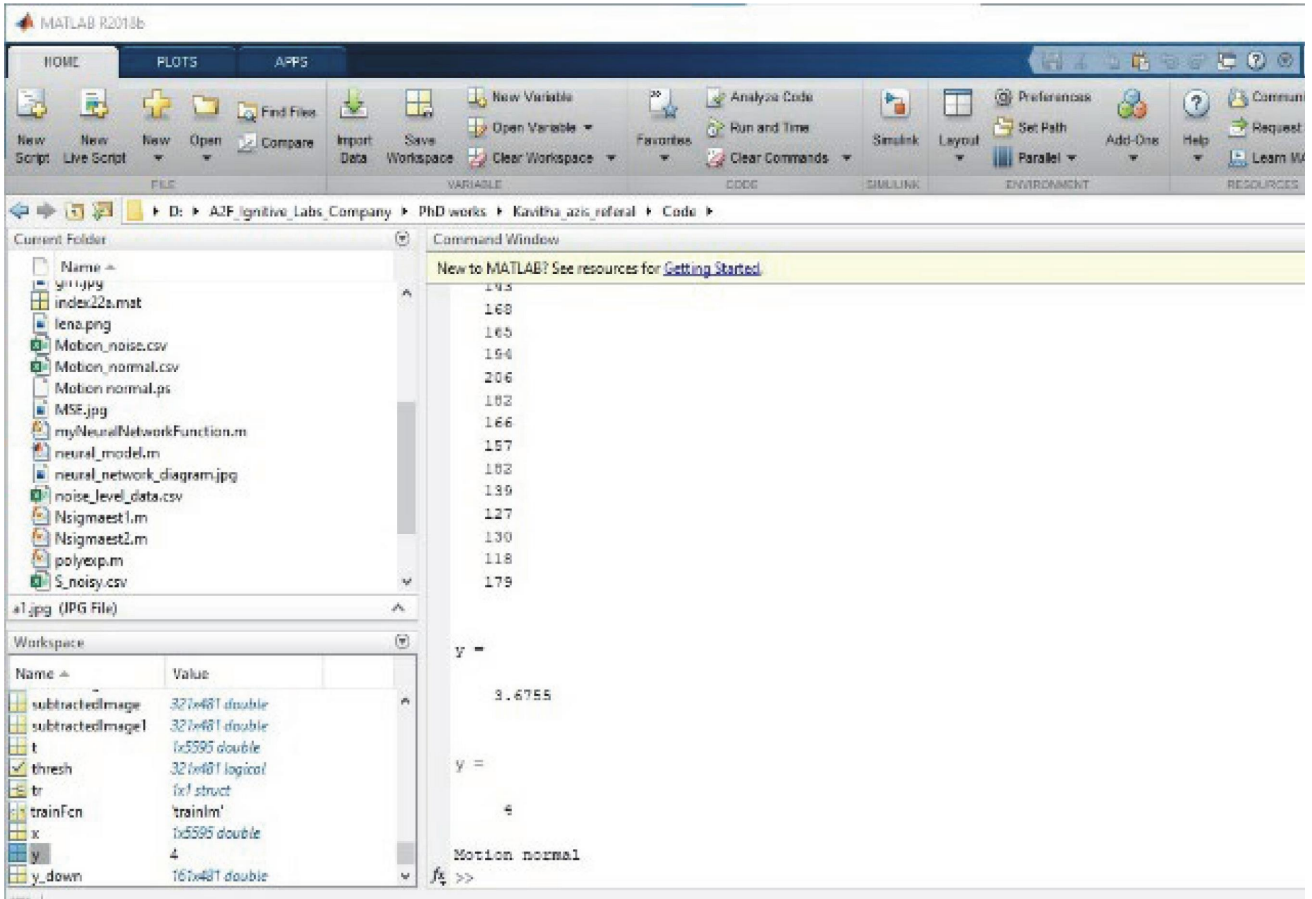
FIGURE 8: Estimated noise.

TABLE 6: Estimated noise level of five noise types.

Noise type	Added noise level	Estimated noise on natural images	Estimated noise on medical images
Gaussian	Mean = 0, variance = 2	280,380	2,687
Motion	Pixels = 15, angle = 20	2,195	1
Poisson	Variance = 0.04	34,311	4,740
Salt-and-pepper	Density = 0.05	71,220	46,740
Speckle	Variance = 0.04	54,126	9,203

The table shows the estimated noise levels for Gaussian is 2,687, motion noise is 1, Poisson noise is 4,740, salt-and-pepper noise is 46,740, and speckle noise is 9,203. From this, it is not possible to corelate the estimated noise level with the added noise.

The visualization of the neural fit model is shown in Figure 7, the input is standard noise calculated from Rician noise equation and the output is fitted using the neural-fitting model [35].

3.6. Noise Type Identification. Instead of directly providing images to CNN model, they are dimensionally reduced by half the size of the image and dimensionally reduced by performing Hadamard multiplication of HH sub-band and downsampled image [36]. Thus, obtained images are of high intensity. Hence, they are considered noise features. These images with noise features are fed to the CNN model for identifying noise types. Each layer of CNN architecture has four convolutional layers with a 3×3 kernel and filters of 8, 16, 32, and 32. Between each convolutional layer, batch normalization, ReLU is applied with max pooling, followed by fitting tool SoftMax with learning rate 1×10^{-4} and 40 validation frequency. The details of every layer are shown in Table 3.

It is known that Convolutional layer performs the convolution operation and Batch Normalization standardizes and normalizes the input from one layer to another. This
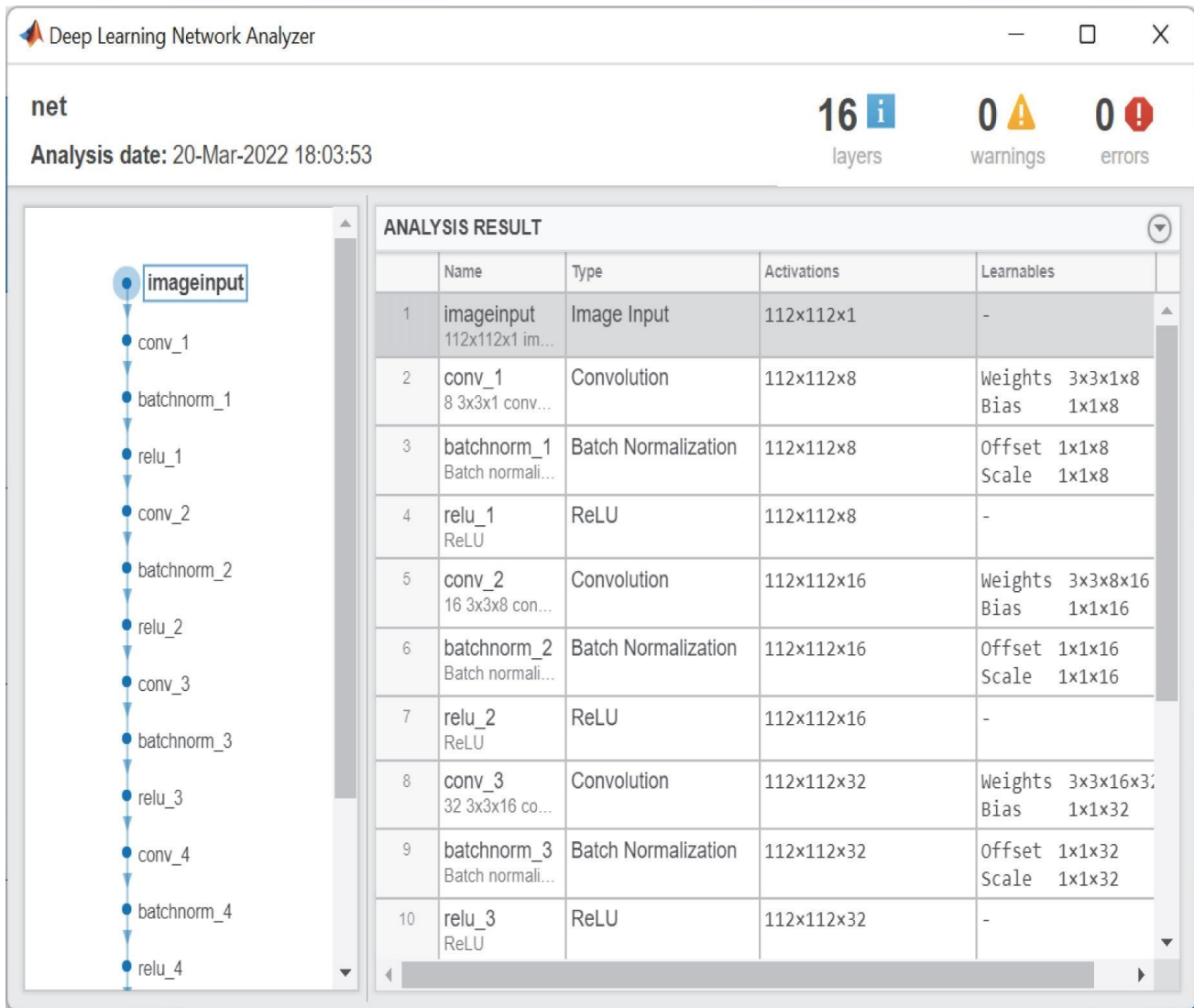
FIGURE 9: Network analyzer for noise type.

helps to reduce the number of epochs [37]. The dimensionality of the feature map is reduced by the pooling layer [38].

4. Results and Discussion

The experiment is run to estimate the noise and to identify the noise type of the given image. Two datasets are used: standard 44 natural images from USC-SIPI image database [34]. The medical images from the cancer imaging archive TCIA [35] and local hospitals are shown in Table 4. These images are noised with Gaussian, motion, Poisson, salt-and-pepper, and speckle. After adding noise, natural images dataset size are 1,100 images and the medical images are 2,890 images. Details of data acquisition are given in Table 4.

Sample images from these databases are shown in Table 5. For experimentation, MATLAB 2019® is used. The dataset is divided into training, testing, and validation set in the ratio of 60 : 20 : 20.

The result and discussion have two subdivisions: noise estimation and noise identification.

4.1. Noise Estimation. The estimated noise level for motion-noised image is shown in Figure 8. The estimated noise level is 3.6755.

The estimated noise for natural and medical images with different noise is shown in Table 6.

4.2. Noise Identification. For noise type identification, CNN model without max pooling layer is used for the proposed methodology (Figure 1). The experiment is carried out on natural images and medical images.

The performance analysis of the defined CNN model to identify the noise is shown in Figure 9. The training process is shown in Figure 10 with validation accuracy of 97.05%.

The confusion matrix for natural images and medical images are shown in Figures 11(a) and 11(b), respectively. This shows the predicted class and the true class.
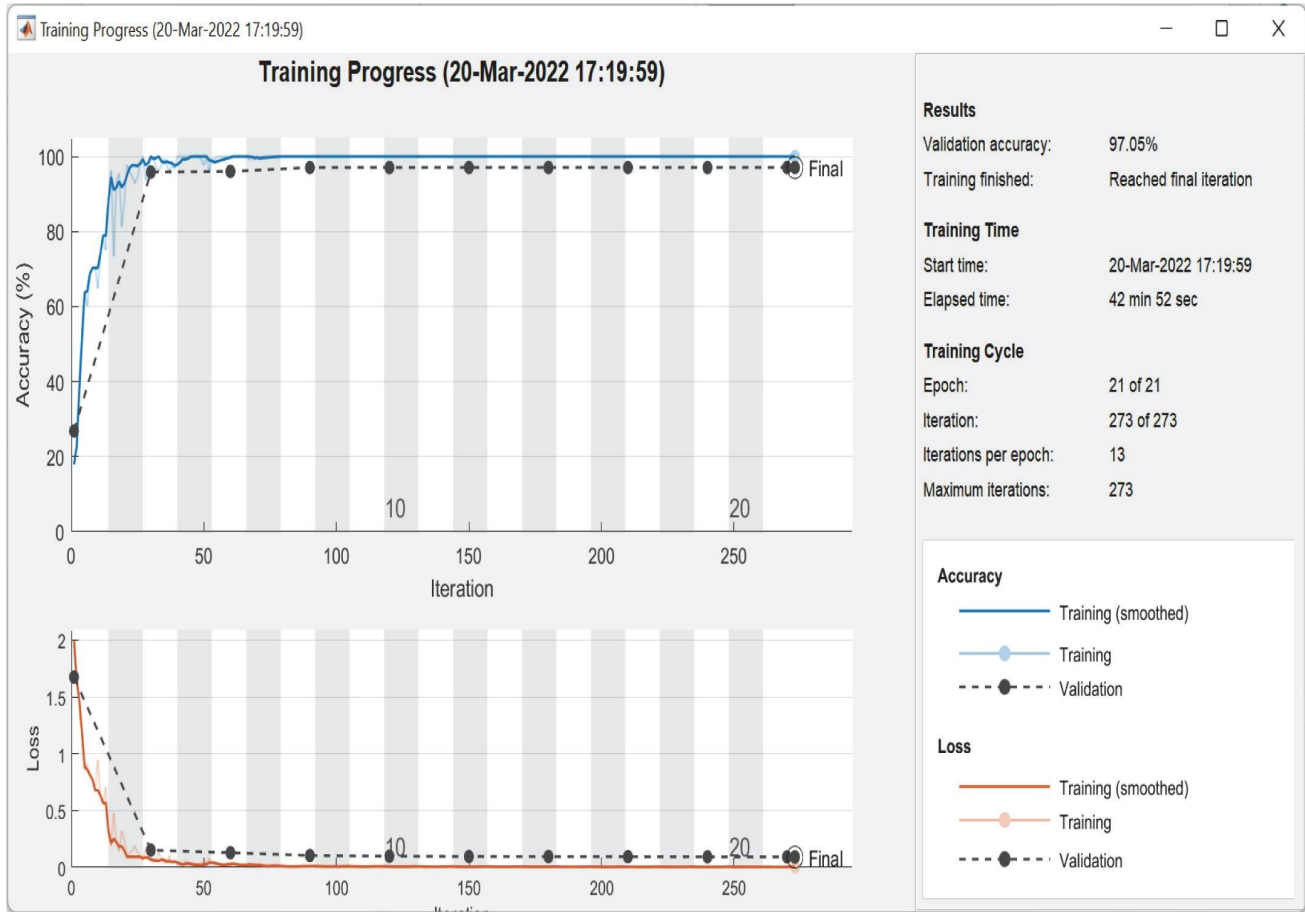
FIGURE 10: Training progress for noise type.

The results of the confusion matrix of natural images show accuracy of 100%. Hence, when we applied the proposed model to the medical images, the results show accuracy of 96.3%. The performance analysis of the proposed system for natural images and medical images is shown in Table 7.

4.2.1. Comparative Study. A comparative study shows the accuracy of the proposed algorithm is more accurate for identifying the noise type present in the natural and medical images as shown in Table 8.

The graph in Figure 12 shows the performance of this algorithm with other methods. The graph shows that this method of CNN using edge-subtracted HH subcomponent has good accuracy compared to other authors' algorithms.

5. Conclusion

The nature of noise type is preassumed based on the imaging modality used. With these assumptions, filters performance is saturated. Hence, an intelligent image noise estimation and noise type recognition method are needed. Once the estimated noise and noise type corrupting an image are identified, an appropriate denoising filter with estimated noise can be applied. For denoising, it is important to characterize the noise type and the estimate noise based on their characteristics of distribution. Here, an experiment was carried out on the dataset of natural images from SIPI and medical images collected from TSIA and local Hospitals. The noises considered for identification are Gaussian, motion, Poisson, salt-and-pepper, and speckle. In the proposed system, instead of using images directly, the only noise component of the image is fed to the CNN for classification. HH sub-band of the DWT transformation has high-intensity values and also edges. From the HH band, edge components are removed by performing Hadamard operation with the Sobel edge-detected downsampled image. For noise estimation, the neural fit model is used, and for classification CNN model. The CNN architecture was designed without max pooling. Experimenting on natural images with five noises gives 100% accuracy, and on medical images with the same five noises gives the accuracy of 96.3%. The images contain multiple noises; hence, in future, the experiment of noise estimation and noise type identification can be carried out on these images. Also, further enhancement can be carried out on different datasets with different noise types.
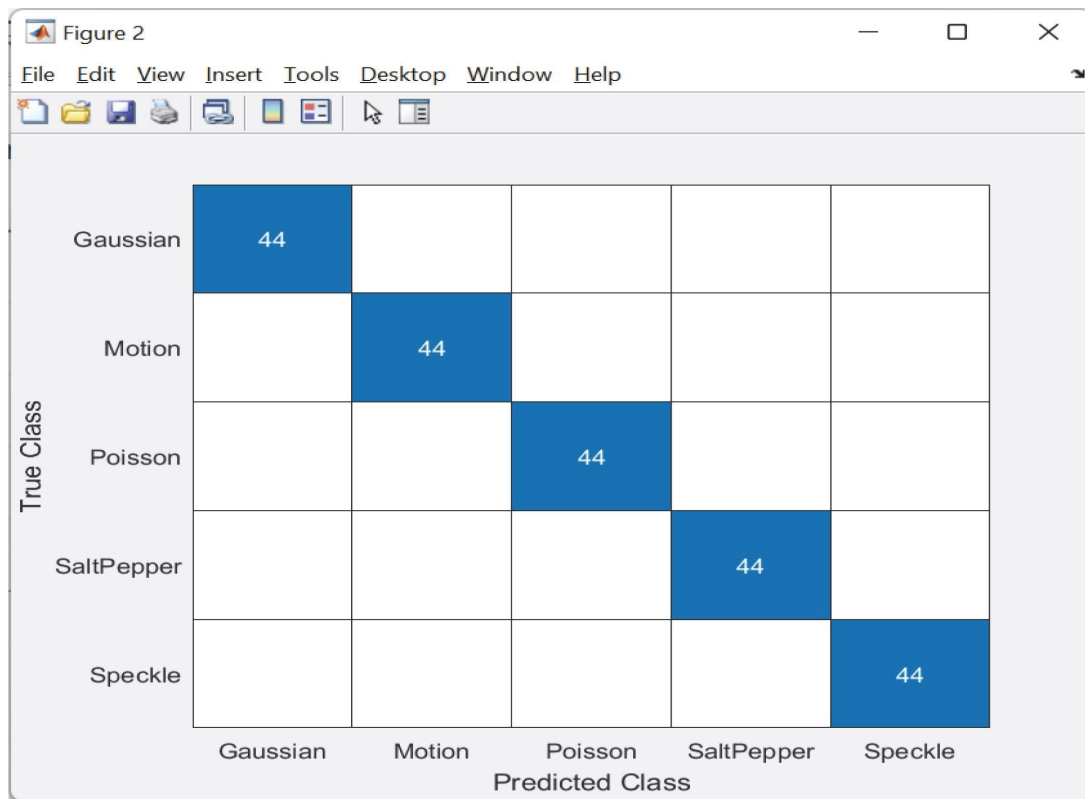
(a)
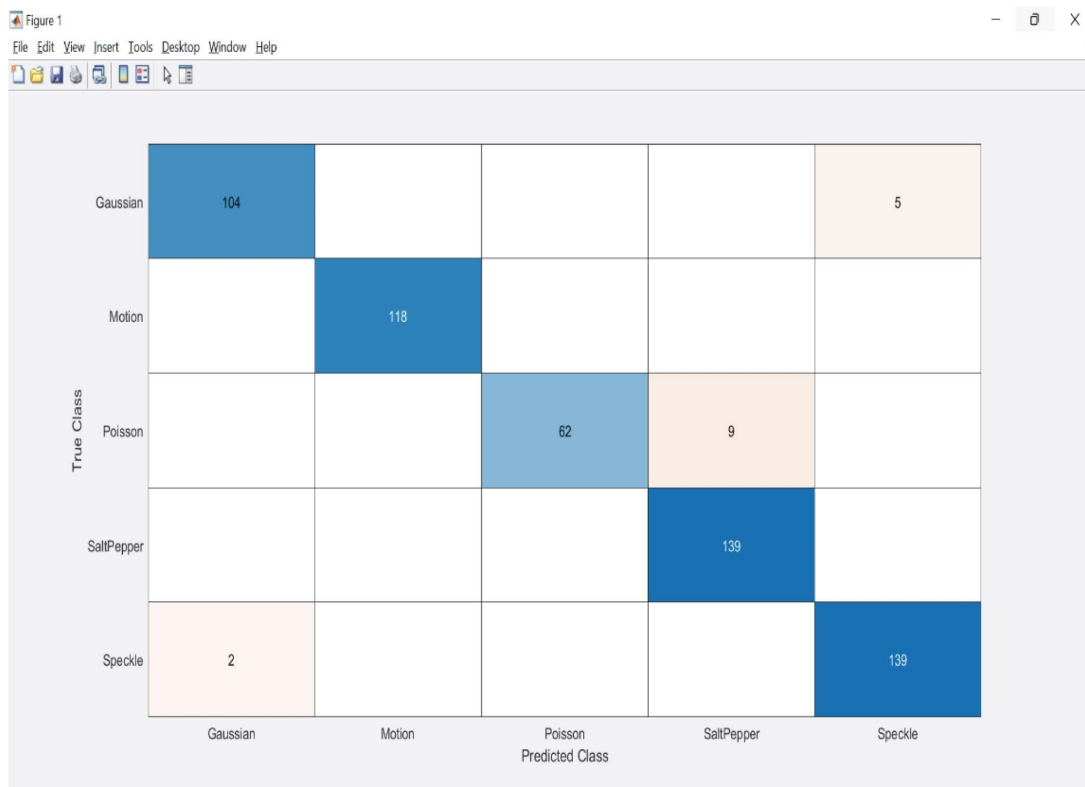
(b)

FIGURE 11: (a) Confusion matrix for noise type identification of natural images; (b) confusion matrix for noise type identification of medical images.

TABLE 7: Performance of noise type identification for natural images and medical images.

	Gaussian	Motion	Poisson	Salt-and-pepper	Speckle	Average
(a) Performance of noise type identification for natural images[a]						
Precision	1.0	1.0	1.0	1.0	1.0	1.0
Recall	1,0	1.0	1.0	1.0	1,0	1.0
F1-score	1.0	1.0	1.0	1.0	1.0	1.0
Accuracy	1.0	1.0	1.0	1.0	1.0	1.0
(b) Performance of noise type identification for medical images[b]						
Precision	0.954	1.0	0.873	1.0	0.986	0.963
Recall	0.981	1.0	1.0	0.939	0.962	0.976
F1-score	0.967	1.0	0.932	0.965	0.974	0.977
Accuracy	0.955	1.0	0.873	1.0	0.986	0.963

[a]This shows the average precision, recall, F1-score, and accuracy is 1.0. [b]This shows the average precision obtained is 0.963 and recall is 0.976. F1-score is 0.977 and accuracy is 0.963.

TABLE 8: Performance of proposed methodology with other authors and algorithms.

| Reference no.	Methodology	Noises considered	Dataset used	Accuracy
[29]	ANN	Impulse and electronic	Natural images	93.75%
[28]	CNN with PCA	Gaussian, salt-and-pepper, speckle, and Poisson	Natural images from SIPI image database–misc	99.3%
[14]	Moment-based classification using kurtosis	Impulse noise	Natural images from SIPI image database–misc	Not given
[32]	NN with moments	Gaussian, speckle, salt-and-pepper	Natural images	ANN 87% and NN 90%
[31]	PNN with kurtosis and skewness	Gaussian, speckle, salt-and-pepper and non-Gaussian	Natural images	84%
AdaBoost	AdaBoost	Gaussian, motion, Poisson, salt-and-pepper, and speckle	Medical images	86.93%
Gaussian Naïve Bayes	Naïve Bayes	Gaussian, motion, Poisson, salt-and-pepper, and speckle	Medical images	86.93%
Bernoulli Naïve Bayes	Naïve Bayes	Gaussian, motion, Poisson, salt-and-pepper, and speckle	Medical images	76.83%
Proposed methodology	CNN with HH sub-band	Gaussian, motion artifacts, Poisson, salt-and-pepper, and speckle.	Natural images from SIPI image database–misc	100%
Proposed methodology	CNN with HH sub-band	Gaussian, motion artifacts, Poisson, salt-and-pepper, and speckle.	Medical images of MRI, CT, and ultrasound	96.3%
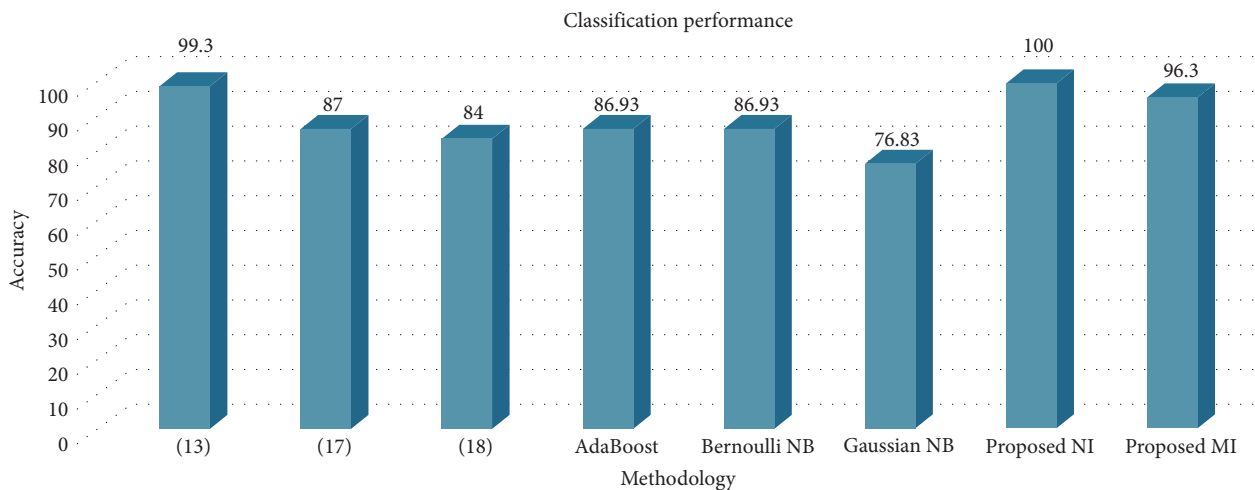
FIGURE 12: Performance noise type identification of proposed methodology with other methods.

Data Availability

The data that support the findings of this study are available on request from the corresponding author.

Conflicts of Interest

The authors declare that they have no conflict of interest.

Funding

References

[1] Ruptured brain aneurysm | Cincinnati, OH Mayfield Brain, and Spine, February 2021, https://mayfieldclinic.com/pe-ane urrupt.htm.

[2] S. Aja-Fernandez, C. Alberola-Lopez, and C.-F. Westin, "Noise and signal estimation in magnitude MRI and Rician distributed images: a LMMSE approach," *IEEE Transactions on Image Processing*, vol. 17, no. 8, pp. 1383–1398, 2008.

[3] S. Aja-Fernández, T. Pieçiak, and G. Vegas-Sánchez-Ferrero, "Spatially variant noise estimation in MRI: a homomorphic approach," *Medical Image Analysis*, vol. 20, no. 1, pp. 184–197, 2015.

[4] H. Gudbjartsson and S. Patz, "The Rician distribution of noisy MRI data," *Magnetic Resonance in Medicine*, vol. 34, no. 6, pp. 910–914, 1995.

[5] D. Singh, V. Kumar, and M. Kaur, "Image dehazing using window-based integrated means filter," *Multimedia Tools and Applications*, vol. 79, pp. 34771–34793, 2020.

[6] A. Buades, B. Coll, and J.-M. Morel, "A non-local algorithm for image denoising," in *2005 IEEE Computer Society Conference on Computer Vision and Pattern Recognition (CVPR'05)*, vol. 2, pp. 60–65, San Diego, CA, USA, 2005.

[7] J. Mohan, V. Krishnaveni, and Y. Guo, "A survey on the magnetic resonance image denoising methods," *Biomedical Signal Processing and Control*, vol. 9, pp. 56–69, 2014.

[8] C. K. Chui, *An Introduction to Wavelets[M]*, pp. 161–171, Xi'an Jiaotong University Press, Xi'an, 1995.

[9] M. Juneja and P. S. Sandhu, "Performance evaluation of edge detection techniques for images in spatial domain," *International Journal of Computer Theory and Engineering*, vol. 1, no. 5, pp. 614–621, 2009.

[10] T. Zin, S. Seta, Y. Nakahara, T. Yamaguchi, and M. Ikhehara, "Local image denoising using RAISA," *IEEE Access*, vol. 10, pp. 22420–22428, 2022.

[11] V. Bhandari, S. Tamrakar, P. Shukla, and A. Bhandari, "A new model of M-secure image via quantization," in *Data, Engineering, and Applications*, R. K. Shukla, J. Agrawal, S. Sharma, and S. Singh Tomer, Eds., Springer, Singapore, 2019.

[12] P. Jiang, Q. Wang, and J. Wu, "Efficient noise level estimation based on principal image texture," *IEEE Transactions on Circuits and Systems for Video Technology*, vol. 30, no. 7, 2020.

[13] V. Shukla, P. Khandekar, and A. Khaparde, "Noise estimation in 2D MRI using DWT coefficients and optimized neural network," *Biomedical Signal Processing and Control*, vol. 71, Part B, Article ID 103225, 2022.

[14] G. Maragatham, S. Md. Mansoor Roomi, and P. Vasuki, "Noise detection in images using moments," *Research Journal of Applied Sciences, Engineering and Technology*, vol. 10, no. 3, pp. 307–314, 2015.

[15] G. Kaur, K. S. Saini, D. Singh, and M. Kaur, "A comprehensive study on computational pansharpening techniques for remote sensing images," *Archives of Computational Methods in Engineering*, vol. 28, pp. 4961–4978, 2021.

[16] G. P. Bhelke, M. V. Sarode, and H. B. Nadiyana, "Detection of noise in degraded images by efficient noise detection algorithm: a survey," *International Joural of Application or Innovations in Engineering & Management (IJAIEM)*, vol. 2, no. 4, 2013.

[17] S. V. Kumar and C. Nagaraju, "Support vector neural network based fuzzy hybrid filter for impulse noise identification and removal from grayscale image," *Journal of King Saud University - Computer and Information Sciences*, vol. 33, no. 7, pp. 820–835, 2021.

[18] G. Papageorgiou, P. Bouboulis, S. Theodoridis, and K. Themelis, "Robust linear regression analysis-the greedy way," in *2014 22nd European Signal Processing Conference (EUSIPCO)*, pp. 16–20, IEEE, Lisbon, Portugal, 2014.

[19] A. E. Ilesanmi and T. O. Ilesanmi, "Methods for image denoising using convolutional neural network: a review," *Complex & Intelligent Systems*, vol. 7, pp. 2179–2198, 2021.

[20] A. Shanmugam and S. R. Devi, "A fuzzy model for noise estimation in magnetic resonance images," *IRBM*, vol. 41, no. 5, pp. 261–266, 2020.

[21] V. A. Pimpalkhute, R. Page, A. Kothari, K. M. Bhurchandi, and V. M. Kamble, "Digital image noise estimation using DWT coefficients," *IEEE Transactions on Image Processing*, vol. 30, pp. 1962–1972, 2021.

[22] Y. Chang, L. Yan, M. Chen, H. Fang, and S. Zhong, "Two-stage convolutional neural network for medical noise removal via image decomposition," *IEEE Transactions on Instrumentation and Measurement*, vol. 69, no. 6, pp. 2707–2721, 2020.

[23] C. Sridhar, P. K. Pareek, R. Kalidoss, S. S. Jamal, P. K. Shukla, and S. J. Nuagah, "Optimal medical image size reduction model creation using recurrent neural network and GenPSOWVQ," *Journal of Healthcare Engineering*, vol. 2022, Article ID 2354866, 8 pages, 2022.

[24] S. Rai, J. S. Bhatt, and S. K. Patra, "An unsupervised deep learning framework for medical image denoising," Senior Member, IEEE. Indian Institute of Information Technology Vadodara, India, 2021.

[25] N. K. Rathore, N. K. Jain, P. K. Shukla, U. S. Rawat, and R. Dubey, "Image forgery detection using singular value decomposition with some attacks," *National Academy Science Letters*, vol. 44, pp. 331–338, 2021.

[26] K. K. Wong, J. S. Cummock, Y. He, R. Ghosh, J. J. Volpi, and S. T. C. Wong, "Retrospective study of deep learning to reduce noise in non-contrast head CT images," *Computerized Medical Imaging and Graphics*, vol. 94, Article ID 101996, 2021.

[27] Y. Li, K. Zhang, W. Shi, Y. Miao, and Z. Jiang, "A novel medical image denoising method based on conditional generative adversarial network," *Computational and Mathematical Methods in Medicine*, vol. 2021, Article ID 9974017, 11 pages, 2021.

[28] H. Y. Khaw, F. C. Soon, J. H. Chuah, and C.-O. Chow, "Image noise types recognition using convolutional neural network with principal components analysis," *IET Image Processing*, vol. 11, no. 12, pp. 1238–1245, 2017.

[29] S. Hiremath and A. S. Rani, "Identification of noise in an image using artificial neural network," *International Journal of Engineering Research and Technology (IJERT)*, vol. 10, no. 2, 2021.

[30] L. Sun and F. Zhong, "Mixed noise estimation for hyperspectral image based on multiple bands prediction," *IEEE Geoscience and Remote Sensing Letters*, vol. 19, Article ID 6007705, 2022.

[31] K. G. Karibasappa, S. Hiremath, and K. Karibasappa, "Neural network-based noise identification in digital images," *The Association of Computer Electronics and Electrical Engineers International Journal on Network Security*, vol. 2, no. 3, pp. 28–31, 2011.

[32] P. Vasuki, C. Bhavana, S. Mohamed Mansoor Roomi, and E. Lakshmi Deebikaa, "Automatic noise identification in images using moments and neural network," in *2012 International Conference on Machine Vision and Image Processing (MVIP)*, pp. 61–64, Coimbatore, India, 2012.

[33] M. Kaur and D. Singh, "Multi-modality medical image fusion technique using multi-objective differential evolution based deep neural networks," *Journal of Ambient Intelligence and Humanized Computing*, vol. 12, pp. 2483–2493, 2021.

[34] https://sipi.usc.edu/database/database.php?volume%E2%80%89=%E2%80%89misc.

[35] K. Clark, B. Vendt, K. Smith et al., "The Cancer Imaging Archive (TCIA): maintaining and operating a public information repository," *Journal of Digital Imaging*, vol. 26, pp. 1045–1057, 2013.

[36] R. Singh, P. Rawat, and P. Shukla, "Robust medical image authentication using 2-D stationary wavelet transform and edge detection," in *2nd IET International Conference on Biomedical Image and Signal Processing (ICBISP 2017)*, Wuhan, China, May 2017.

[37] R. Singh, P. Shukla, P. Rawat, and P. K. Shukla, "Invisible medical image watermarking using edge detection and discrete wavelet transform coefficients," *International Journal of Innovative Technology and Exploring Engineering (IJITEE)*, vol. 9, no. 1, pp. 5074–5580, 2019.

[38] P. Subashini and P. T. Bharathi, "Automatic noise identification in images using statistical features," *International Journal for Computer Science and Technology*, vol. 2, no. 3, pp. 467–471, 2011.